LETTER • OPEN ACCESS

Cooling flow regime of a plasma thermal quench

To cite this article: Yanzeng Zhang *et al* 2023 *EPL* **141** 54002

A Letters Journal Exploring the Frontiers of Physics

March 2023

EPL, **141** (2023) 54002
doi: 10.1209/0295-5075/acbb20

www.epljournal.org

Cooling flow regime of a plasma thermal quench

Yanzeng Zhang[1(a)], Jun Li[1,2] and Xian-Zhu Tang[1]

[1] *Theoretical Division, Los Alamos National Laboratory - Los Alamos, NM 87545, USA*
[2] *School of Nuclear Science and Technology, University of Science and Technology of China - Hefei, Anhui, China*

received 22 November 2022; accepted in final form 10 February 2023
published online 22 February 2023

Abstract – A large class of Laboratory, Space, and Astrophysical plasmas is nearly collisionless. When a localized energy or particle sink, for example, in the form of a radiative cooling spot or a black hole, is introduced into such a plasma, it can trigger a plasma thermal collapse, also known as a thermal quench in tokamak fusion. Here we show that the electron thermal conduction in such a nearly collisionless plasma follows the convective energy transport scaling in itself or in its spatial gradient, due to the constraint of ambipolar transport. As a result, a robust cooling flow aggregates mass toward the cooling spot and the thermal collapse of the surrounding plasma takes the form of four propagating fronts that originate from the radiative cooling spot, along the magnetic field line in a magnetized plasma. The slowest one, which is responsible for deep cooling, is a shock front.

Introduction. – A signature property of a large class of magnetized and unmagnetized plasmas in the Laboratory, Space, and Astrophysical systems is the extremely low collisionality that can be due to high plasma temperature T_e or low plasma density n_e, or a combination of the two [1]. For example, a fusion-grade plasma in a tokamak reactor has $T_e \sim$ 10–20 kiloelectronvolts (keV) and $n_e \sim 10^{19\text{–}20}$ per cubic meter, which results in a mean free path $\lambda_{mfp} \sim 10^4$ meters (m), while the toroidal length of the confinement chamber is merely 20–30 m [2–4]. In the Earth's radiation belt, the electron λ_{mfp} can be as long as 10^{11} m or higher with huge variations in electron energy and density [5–8]. At the even greater scale of clusters of galaxies, the intracluster hot gas has $n_e \sim 10^2$–$10^4\,\mathrm{m}^{-3}$ and $T_e \sim 2\times10^7$–10^8 K [9–13], so λ_{mfp} is in the order of tens of kiloparsec to megaparsec.

A whole class of problems arises if a localized cooling spot is introduced into such a nearly collisionless plasma. This could be structure formation in a galaxy cluster where a radiative cooling spot is driven by increased particle density [9] or an event horizon of a black hole that provides an absorbing boundary for plasmas [14]. A satellite traversing the Earth's radiation belt can be a sink for plasma energy and particles [15,16]. In a tokamak reactor, solid pellets that are injected into the fusion plasma for fueling and disruption mitigation [17–20], provide localized cooling due to a combination of energy spent on phase transition and ionization of the solid materials, and the radiative cooling that is especially strong when high-Z impurities are embedded in the frozen pellet. Even in the absence of pellet injection, large-scale magnetohydrodynamic instabilities can turn nested flux surfaces into globally stochastic field lines that connect fusion core plasma directly onto the divertor/first wall [21–24], causing a thermal collapse via fast parallel transport along the field lines within a short period of time that can range from microseconds to milliseconds [25]. Notice that the high-Z impurities originated from the divertor region can migrate to the core region and cool the plasma in both regions via radiations, *e.g.*, see ref. [26]. An outstanding physics question is how a thermal collapse of the surrounding plasma, commonly known as a thermal quench in tokamak fusion, would come about in such a diverse range of applications.

The most obvious route for the thermal collapse is via electron thermal conduction along the magnetic field line that intercepts the cooling spot, for which the Braginskii formula [27] would produce an enormous heat flux [9,11] if there is a sizeable temperature difference $\Delta T = T_0 - T_w \sim T_0$ between the cooling spot (T_w) and surrounding plasmas (T_0),

$$q_{e\parallel} = n_e\chi_e\hat{\mathbf{b}}\cdot\nabla T_e \sim n_e v_{th,e}\frac{\lambda_{mfp}}{L_T}\Delta T \sim n_e v_{th,e}\frac{\lambda_{mfp}}{L_T}T_0. \quad (1)$$

(a) E-mail: yzengzhang@lanl.gov (corresponding author)

Here $q_{e\parallel}$ is the parallel electron conduction heat flux, χ_e the thermal conductivity, $\hat{b}$ the unit vector in the magnetic field direction, $v_{th,e} = \sqrt{T_0/m_e}$ the electron thermal speed, and L_T the distance or field line length over which ΔT is established. For a nearly collisionless plasma, the temperature collapse necessarily starts with Knudsen number $K_n \equiv \lambda_{mfp}/L_T \gg 1$, a regime in which the free-streaming limit [28] of

$$q_{e\parallel} \approx \alpha n_e v_{th,e} T_0, \tag{2}$$

is supposed to apply in lieu of Braginskii, with $\alpha \approx 0.1$ [29].

The pressure-gradient–driven plasma flow $V_{i\parallel}$ along the magnetic field line is limited by the ion sound speed c_s, so the convective electron energy flux is bounded by $n_e c_s T_0$. Equation (2) suggests that the electron energy flux would be dominated by conduction as normally $v_{th,e} \gg c_s$ in a plasma of comparable electron and ion temperatures. In such a conduction-dominated situation, the much colder but denser cooling spot would be rapidly heated up by the electron thermal conduction from the surrounding hot plasma, and as a result, it can become over-pressured and the original cooling spot, say an ablated pellet in a tokamak, tends to expand into the surrounding plasma, yielding an outflow.

In the aforementioned problem of clusters of galaxies, one has instead observed robust cooling flows into the radiative cooling spot that aggregate mass onto the cooling spot [9], although more recent observations reveal a more modest mass-accreting cooling flow that indicates the role of various additional heating mechanisms to balance the cooling [11–13]. This is inconsistent with the conduction-dominated scenario mentioned above [9,11,30,31]. Extensive efforts have been made to find ways to inhibit the electron thermal conduction in the nearly collisionless plasma, for example, by tangled magnetic fields [32,33] or plasma instabilities [34–36], in order to reach the convection-dominated scenario, which would naturally yield the *cooling flow regime* of a plasma thermal quench.

In this letter, we show that in a nearly collisionless plasma, even along the magnetic field lines, like in the case of pellet injection into a tokamak, ambipolar transport will naturally constrain the electron parallel thermal conduction in such a way that the plasma thermal collapse comes with a cooling flow toward the radiative cooling spot. The necessary constraint is on the spatial gradient of electron parallel conduction flux, which can be seen from the energy equation for the electrons along the magnetic field,

$$n_e \left(\frac{\partial}{\partial t} T_{e\parallel} + V_{e\parallel} \frac{\partial}{\partial x} T_{e\parallel} \right) + 2 n_e T_{e\parallel} \frac{\partial}{\partial x} V_{e\parallel} + \frac{\partial}{\partial x} q_{en} = 0. \tag{3}$$

Here x is the distance along the magnetic field line, $n_e, T_{e\parallel}, V_{e\parallel}$ are the density, parallel temperature, and parallel flow of the electrons, and $q_{en} \equiv \int m_e (\mathbf{v}_\parallel - V_{e\parallel})^3 f_e \mathrm{d}^3\mathbf{v}$ is a component of the parallel heat flux. Let the cooling flow span a length L_T, one can see the convective energy transport terms follow the scaling of $n_e T_{e\parallel} V_{e\parallel}/L_T$. Ambipolar transport constrains $V_{e\parallel} \approx V_{i\parallel} \propto m_i^{-1/2}$, so the free-streaming scaling of q_{en} in eq. (2) would predict $\partial q_{en}/\partial x \sim \alpha n_e v_{th,e} T_{e\parallel}/L_T \propto m_e^{-1/2}$, which would overwhelm the convective energy transport ($\propto m_i^{-1/2}$) to force a $T_{e\parallel}$ collapse and remove the pressure gradient drive that sustains the cooling flow. The condition for accessing the cooling flow regime of plasma thermal quench is thus

$$\frac{\partial q_{en}}{\partial x} \sim n_e T_{e\parallel} V_{i\parallel}/L_T, \tag{4}$$

and it is violated by both eq. (1) and eq. (2), two most commonly used heat flux closures in fluid codes. We report in this letter that the condition of eq. (4) is indeed realized by ambipolar constraint in a nearly collisionless plasma, a constraint that has found important implications in fusion plasmas (*e.g.*, see [37–41]). In the case that the cooling spot is a perfect particle and energy sink (*e.g.*, a black hole), which can be modeled by an absorbing boundary, q_{en} itself obtains the convective energy transport scaling, $q_{en} \sim n_e V_{i\parallel} T_{e\parallel}$. With a radiative cooling mass, which can be modeled as a thermobath, the boundary of which recycles all particles across the boundary but clamps the temperature to a low value $T_w \ll T_0$, the cold electrons thus produced can restore the free-stream scaling for $q_{en} \sim \alpha n_e v_{th,e} T_{e\parallel}$ but its spatial gradient over the cooling flow region retains the convective energy transport scaling of eq. (4). As a result, a robust cooling flow appears to aggregate mass towards the cooling spot.

Methods. – We deployed fully kinetic simulations using the VPIC [42] code to investigate the thermal collapse of a nearly collisionless plasma in the presence of a cooling spot, where the parallel transport physics will dominate. The simplest problem setup to decipher the parallel cooling physics is to unwind the open field lines into a one-dimensional slab with length L_x, where a cooling spot is introduced at the left boundary and the right boundary is effectively at infinity. The cooling spot is implemented as either a thermobath (for a radiative cooling spot) or an absorbing boundary (for a sink of both energy and particles), where the former conserves particles by re-injecting electron-ion pairs (equal to the ions across the boundary) with a clamped temperature $T_w \ll T_0$. The boundary simply reflects the particles so it does not change the plasma particle number nor the plasma energy. In such a semi-infinite collisionless plasma, there is no characteristic length except for the Debye length λ_D that must be resolved in VPIC simulations. Therefore, we choose the resolution of the grid as $\mathrm{d}x = 0.1\lambda_D$ with 5000 markers per cell. This simulated "infinity" right boundary would not affect the plasma cooling dynamics as long as the electron precooling front (defined later) has not reached the simulation boundary on the right side.

Results. – Most interestingly, in such a cooling flow regime, the plasma thermal collapse comes in the form

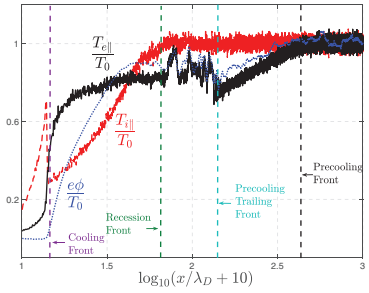

Fig. 1: Normalized parallel electron and ion temperature, and electrostatic potential at $\omega_{pe}t = 176$ for $T_w = 0.01T_0$ from first-principle VPIC simulations. Different right-going fronts are labeled, where a uniform plasma with constant temperature T_0 and density n_0 initially fills the whole domain $x \in [0, 1500\lambda_D]$ with λ_D the Debye length. The simulation uses a reduced ion mass of $m_i = 100m_e, \delta x = 0.1\lambda_D$, and 5000 markers per cell. The boundary conditions are explained in the text. Notice that the electrostatic potential plotted here is directly integrated from the instantaneous electric field that contains large amplitude Langmuir waves, which thus is only used as a guide for the qualitative behavior of the quiescent ambipolar potential.

of propagating fronts that originate from the cooling spot with characteristic speeds. There are in total four (three) propagating fronts for the thermobath (absorbing) boundary: two of them propagate at speeds that scale with $v_{th,e}$, so are named *electron fronts*, while the other two are *ion fronts* that propagate at speeds that scale with the local ion sound speed c_s (the last ion front disappears for the absorbing boundary). Figure 1 illustrates the structure of the four fronts that propagate into a hot plasma (T_0) for the thermal collapse with a thermobath boundary ($T_w \ll T_0$). We notice that the results from collisionless plasma simulation with $\lambda_{mfp} \to \infty$ are similar to those in nearly collisionless plasma with $\lambda_{mfp} \gg L_x$ so only the former are used in the letter. It is important to note that cooling of a nearly collisionless plasma produces a strong temperature anisotropy, so one must examine the collapse of $T_\|$ and $T_\perp$ separately.

Electron fronts. Cooling of $T_{e\|}$ in a nearly collisionless plasma is primarily through free-streaming loss of suprathermal electrons satisfying $v_\| < -\sqrt{2e(\Delta\Phi)_{max}/m_e}$ into the radiative cooling spot. Here $(\Delta\Phi)_{max}$ is the maximum reflective potential in the plasma with $\Delta\Phi = \Phi_\infty - \Phi(x)$ and the constant Φ_∞ the far upstream plasma potential. The precooling zone bounded by the precooling front (PF) and the precooling trailing front (PTF) has $T_{i\|}$ unchanged and $V_{i\|} \approx 0$, but a lowered $T_{e\|}$, which is due to the depletion of fast electrons satisfying $v_\| > v_c = \sqrt{2e\left[(\Delta\Phi)_{max} - \Delta\Phi\right]/m_e}$, yielding a truncated Maxwellian

$$f_e(v_\|, v_\perp) = \frac{n_m\left(\Phi(x)\right)}{\sqrt{2\pi}v_{th,e}^3} e^{-\left(v_\|^2+v_\perp^2\right)/2v_{th,e}^2}\Theta\left(1 - \frac{v_\|}{v_c}\right) + \frac{n_b}{2\pi v_\perp}\delta(v_\perp)\delta(v_\| - v_c), \tag{5}$$

with $\Theta(1 - v_\|/v_c)$ the Heaviside step function that vanishes for $v_\| > v_c$, and $\delta(x)$ the Dirac delta function. The ambipolar electric field can draw some low-energy electrons to compensate for the loss of high-energy electrons and thus maintain quasi-neutrality. This in-falling cold electron population is modeled in eq. (5) as a cold beam that due to ambipolar electric field acceleration has the speed v_c (see appendix). Between the PF and PTF, the electron beam can be ignored, so

$$T_{e\|}(v_c) = \frac{\int m_e\tilde{\mathbf{v}}_\|^2 f_e \mathrm{d}\mathbf{v}}{\int f_e \mathrm{d}\mathbf{v}} \approx T_0\left[1 - \frac{v_c}{\sqrt{2\pi}v_{th,e}} e^{-v_c^2/2v_{th,e}^2}\right], \tag{6}$$

where $\tilde{\mathbf{v}}_\| \equiv \mathbf{v}_\| - \mathbf{V}_{e\|}$.

Equation (6) predicts a detectable decrease in $T_{e\|}(v_c)$ from T_0 for $v_c \approx 2.4v_{th,e}$ ($T_{e\|} \approx 0.95T_0$) considering the PIC noise, suggesting an electron PF propagating at

$$U_{PF} = 2.4v_{th,e}. \tag{7}$$

This corresponds to fast electrons with $v_\| > U_{PF}$ traveling from the left boundary into the plasma, leaving behind a distribution at the PF with a void in $v_\| > U_{PF}$. The PTF comes about due to the reflecting potential $(\Delta\Phi)_{RF} = (\Delta\Phi)_{max} - (\Phi_\infty - \Phi_{RF})$ with Φ_{RF} the ambipolar potential at the ion recession front (RF), which sets a lower cutoff speed v_c at

$$U_{PTF} \equiv \sqrt{2e\left(\Delta\Phi\right)_{RF}/m_e}. \tag{8}$$

The deeper void now gives rise to a further reduced $T_{e\|}$,

$$T_{e\|}(U_{PTF}) \approx T_0\left[1 - \sqrt{\frac{e\left(\Delta\Phi\right)_{RF}}{\pi T_0}} e^{-e(\Delta\Phi)_{RF}/T_0}\right]. \tag{9}$$

The PTF rides these electrons that are reflected by the reflecting potential, and propagates at $U_{PTF}(< U_{PF})$. Since the ambipolar reflecting potential must satisfy $e\left(\Delta\Phi\right)_{RF} \sim T_0$ in a nearly collisionless plasma, $U_{PTF} \sim v_{th,e}$ and $T_{e\|}(U_{PTF})$ is only mildly cooler than T_0. Furthermore, $T_{e\|}$ and Φ *vary little* between the RF and PTF, since the cutoff velocity remains the same at U_{PTF}.

The ion flow remains vanishingly small ahead of the RF, so the electron cooling between the RF and PF is the result of electron conduction, which for the model f_e in eq. (5) with $v_c > v_{th,e}$ takes the form

$$q_{en} \approx -\frac{n_m v_{th,e} T_0}{\sqrt{2\pi}}\left(\frac{v_c^2}{v_{th,e}^2} - 1\right) e^{-v_c^2/2v_{th,e}^2} + \frac{n_b T_0 v_c^3}{v_{th,e}^2}. \tag{10}$$

Between PTF and PF, $n_b \approx 0$ and $U_{PTF} \le v_c \le U_{PF}$ so q_{en} does scale as the free-streaming limit of eq. (2), but with α modulating in space as a function of v_c. In fact, for $v_c > \sqrt{2}v_{th,e}$, one finds

$$\frac{\mathrm{d}q_{en}}{\mathrm{d}x} \approx n_m v_c \frac{\partial T_{e\|}}{\partial x}, \tag{11}$$

so the solution of the energy equation, $\partial T_{e\|}/\partial t = -v_c \partial T_{e\|}/\partial x$, reveals that v_c is the recession speed of $T_{e\|}$, re-affirming the particle picture noted earlier that the momentum space void in f_e propagates upstream with a speed of v_c. This large q_{en} drives fast propagating electron fronts (PF and PTF) but produces modest amount of $T_{e\|}$ cooling for the large cutoff speed $v_c = U_{PTF}$.

Ion fronts. Much more aggressive cooling would need to occur as the plasma approaches the radiative cooling spot that is clamped at $T_w \ll T_0$. These are facilitated by the ion fronts that provide the reflecting potential $(\Delta\Phi)_{RF}$. The RF is where $n_i \approx n_e$ starts to drop, and behind which plasma pressure gradient drives a cooling flow toward the radiative cooling spot. The main reflection potential, which is tied to the electron pressure gradient, is also behind the ion RF. An ion recession layer bounded by the RF and the cooling front (CF) is similar to the rarefaction wave formed in the cold plasma interaction with a solid surface [43,44], where the plasma parameters recede steadily with the local sound speed. What is different for the thermal quench of a nearly collisionless plasma is the large plasma temperature and pressure gradient and the nature of the heat flux. The electron flow associated with f_e of eq. (5) within the recession layer is

$$n_e V_{e\|}(v_c) = -\frac{n_m v_{th,e}}{\sqrt{2\pi}} e^{-v_c^2/2v_{th,e}^2} + n_b v_c, \qquad (12)$$

where $n_e(v_c) = \left[1 + \mathrm{Erf}\left(v_c/\sqrt{2}v_{th,e}\right)\right] n_m/2 + n_b$ with Erf(x) being the error function. For an absorbing boundary ($n_b = 0$), a cutoff speed around $v_{th,e}, v_c \approx v_{th,e}\sqrt{2\ln(v_{th,e}/V_{i\|})}$ is sufficient to produce a $V_{e\|}$ that matches onto the increasing ion flow, $V_{e\|} \approx V_{i\|}$, for ambipolar transport through the recession layer. The infalling cold electron beam reduces v_c and hence produces a lower reflecting potential across the recession layer as elucidated in eq. (12).

The physics of q_{en} in the *recession layer* can be elucidated by rewriting eq. (10) as

$$q_{en} = \left(\frac{v_c^2}{v_{th,e}^2} + 2\right) n_e V_{e\|} T_0 - 2 n_b v_c T_0 - 3 n_e T_{e\|} V_{e\|} - n_e m_e V_{e\|}^3. \qquad (13)$$

For an absorbing wall, $n_b = 0$, and one finds q_{en} itself has a convective energy transport scaling: $q_{en} \sim n_e V_{e\|} T_0$. The condition for the cooling flow regime, eq. (4), is obviously satisfied. In the case of a radiative cooling spot that produces a copious amount of cold electrons, the leading order of $q_{en} \sim -2 n_b v_c T_0 \propto n_b v_{th,e} T_0$ follows the free-streaming limit of eq. (2). Remarkably the plasma thermal quench still produces a cooling flow, in which case eq. (4) is satisfied due to the collisionless cold beam in the ambipolar electric field follows flux conservation $n_b v_c = \mathrm{const}$, so $\partial(-2 n_b v_c T_0)/\partial x = 0$ and the remaining terms in q_{en} have convective energy transport scaling. The VPIC [42] kinetic simulations shown in fig. 2 confirm that convective scaling of eq. (4) holds in the recession layer. In other words, electron cooling in a nearly collisionless plasma is modified by ambipolarity in such a way that large $T_{e\|}$ gradient can be supported in the recession layer to drive a cooling flow.

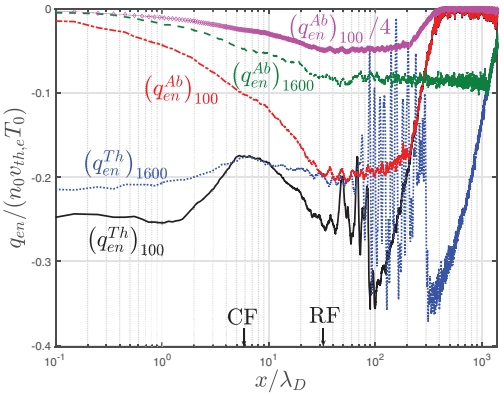

Fig. 2: Electron heat flux q_{en} for different m_i/m_e and boundary conditions at $\omega_{pi}t = 13.6$. The superscripts Ab and Th denote the absorbing and thermobath boundaries at $x = 0$, respectively, while the subscripts 100 and 1600 label $m_i/m_e = 100$ and 1600. For the absorbing boundary, q_{en} behind the recession front (RF) follows the convective scaling by itself, which can be seen by comparing $\left(q_{en}^{Ab}\right)_{1600}$ and $\left(q_{en}^{Ab}\right)_{100}/4$ (notice that their small difference, as seen from eq. (13) for $n_b = 0$, comes from the dependence of $v_c \approx v_{th,e}\sqrt{2\ln(v_{th,e}/V_{i\|})}$ on m_i). For the thermobath boundary, q_{en} recovers the free-streaming formula, but its spatial gradient within the cooling flow region, which is between the cooling front (CF) and the RF, follows the convective scaling, as illustrated by the same slope of the curve as that for the absorbing boundary when m_i/m_e is fixed.

The propagation speed of the RF can be understood by examining the ion dynamics in the recession layer [45–48],

$$\frac{\partial}{\partial t} n_i + \frac{\partial}{\partial x}\left(n_i V_{i\|}\right) = 0, \qquad (14)$$

$$m_i n_i \left(\frac{\partial}{\partial t} V_{i\|} + V_{i\|}\frac{\partial}{\partial x} V_{i\|}\right) + \frac{\partial}{\partial x}(p_{i\|} + p_{e\|}) = 0, \qquad (15)$$

$$n_i \left(\frac{\partial}{\partial t} T_{i\|} + V_{i\|}\frac{\partial}{\partial x} T_{i\|}\right) + 2 n_i T_{i\|}\frac{\partial}{\partial x} V_{i\|} + \frac{\partial}{\partial x} q_{in} = 0, \qquad (16)$$

where we invoked the electron force balance $e n_e E_{\|} \approx -\partial p_{e\|}/\partial x$ and quasi-neutrality $n_e = Z n_i$ with Z the ion charge, and $p_{i,e\|} = n_{i,e} T_{i,e\|}$. Introducing a parameterization of $q_{in} \approx \sigma_i n_i V_{i\|} T_{i\|}$, which is known from [49], and $\partial q_{en}/\partial x \approx \sigma_e \partial\left(n_e V_{e\|} T_{e\|}\right)/\partial x$ from eq. (4), where $\sigma_{e,i} \sim 1$ are analogous to the energy transmission coefficients, we obtain an universal length scale for $p_{e,i\|}$,

$$\frac{\mathrm{d}\ln p_{e\|}}{\mathrm{d}x} \approx \mu \frac{\mathrm{d}\ln p_{i\|}}{\mathrm{d}x}, \qquad (17)$$

where $\mu = (3+\sigma_e)/(3+\sigma_i) \times [-U + (1+\sigma_i)V_{i\|}]/[-U + (1+\sigma_e)V_{i\|}]$. It is interesting to note that $U > 0$ and $V_{i\|} < 0$ have opposite sign in the recession layer where a cooling flow resides. As a result, eqs. (14)–(16) have self-similar

solutions with similarity variable $\xi = x - Ut$ with U being the local recession speed. We find

$$U = [\sigma_i^2 V_{i\|}^2/4 + (1+\sigma_i/3)c_s^2]^{1/2} + (1+\sigma_i/2)V_{i\|}, \quad (18)$$

where $c_s = \sqrt{3(\mu Z T_{e\|} + T_{i\|})/m_i}$ is the local sound speed of a nearly collisionless plasma with anisotropic temperatures. At the ion recession front, $V_{i\|} \approx 0$, so the speed of the ion recession front is

$$U_{RF} = \sqrt{1+\sigma_i/3}c_s. \quad (19)$$

For $Z = 1$, $\sigma_i = 1$, $\mu = 1$ and $T_{e\|} \approx T_{i\|} = T_0$ at the recession front, we have $U_{RF} \approx 2.8 v_{th,i}$ with $v_{th,i} = \sqrt{T_0/m_i}$ the ion thermal speed, which agrees well with the simulation result. It is worth noting that the self-similar solution of eq. (18) also recovers a known constraint [50] on the plasma exit flow at an absorbing boundary where a non-neutral sheath forms. The sheath entrance cannot propagate further upstream in this case so $U = 0$, by which eq. (18) predicts an ion exit flow speed

$$V_{i\|} = -\sqrt{\frac{1+\sigma_i/3}{1+\sigma_i}}c_s \equiv -\sqrt{(\beta 3 Z T_{e\|} + 3T_{i\|})/m_i}, \quad (20)$$

with

$$\beta = \frac{1 - \frac{1}{Ze\Gamma_i}\frac{\partial q_{in}}{\partial \phi}}{1 + \frac{1}{e\Gamma_e}\frac{\partial q_{en}}{\partial \phi}}, \quad (21)$$

and $\Gamma_{e,i} = n_{e,i} V_{e,i\|}$. This is consistent with the Bohm criterion for plasma in steady state ($\mathrm{d}/\mathrm{d}t = 0$) when including the heat flux in the transport model [50].

In the absence of an absorbing boundary, the mass aggregated by the cooling flow will pile up, and the resulting back-pressure can now drive a second ion front (cooling front, CF). Behind the CF, $T_{e\|}$ equilibrates with T_w as shown in fig. 3. Such a deep cooling of $T_{e\|}$ is through thermal conduction as indicated in fig. 2. When the cooling flow runs into this nearly static plasma, the ion flow energy, which is substantial in the cooling flow, is converted into ion thermal energy via a plasma shock as shown in fig. 3. Matching the conserved quantities across the shock while ignoring the heat flux, we find that the speed of the shock, which propagates upstream into the plasma, is simply the upstream sound speed at the shock front. The CF is the shock front, so its speed is

$$U_{CF} = c_s(x = x_{CF}). \quad (22)$$

Since the plasma temperature at the CF is considerably lower than that at the RF, we have $U_{CF} < U_{RF}$. Generally, the colder T_w, the smaller U_{CF}. The presence of the CF and the cooling zone behind it is of fundamental importance to $T_{i\perp}$ and $T_{e\perp}$ cooling as the cold particles provide dilutional cooling. It is also the source of cold electrons that are accelerated by the ambipolar electric field into the recession layer and beyond, cooling down $T_{e\perp}$ further upstream.

Discussions. – In summary, the thermal collapse of a nearly collisionless plasma due to its interaction with a localized particle or energy sink is associated with a cooling flow toward the cooling spot. This applies to unmagnetized plasmas, for example, in astrophysical systems, and magnetized plasmas, for example, in Earth's magnetosphere or a tokamak fusion plasma. It is the fundamental constraint of ambipolar transport, along the field line in a magnetized plasma, that limits the spatial gradient of electron (parallel) heat flux to the much weaker convective ($V_{e\|}$) scaling as opposed to the free-streaming ($v_{th,e}$) scaling. Such weaker scaling is essential to sustain a temperature and hence pressure gradient for driving the cooling flow toward the cooling spot over the ion recession layer. The cooling flow eventually terminates against the cooling spot via a plasma shock that converts the ion flow energy into ion thermal energy. This shock or cooling front propagates away from the cooling spot at upstream ion sound speed, and it has the most profound role in the deep cooling of the surrounding hot plasmas, especially the ions. Unlike the ions, the electrons can be cooled ahead of the recession front due to an electron heat flux that follows the free-streaming limit ($q_{en} \propto n_e v_{th,e} T_e$). Interestingly this large heat flux does not imply significant cooling of $T_{e\|}$ in a nearly collisionless plasma ahead of the recession front, but induces a very limited amount of $T_{e\|}$ drop over a very large volume, because the precooling and precooling trailing fronts have propagation speeds that scale with electron thermal speed.

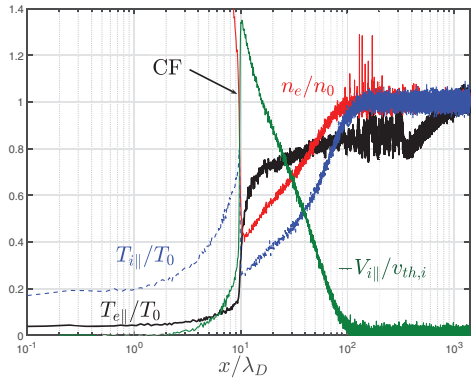

Fig. 3: Plasma profiles corresponding to fig. 1. The jumps near the cooling front (CF) are illustrated, where the huge plasma density near the radiative cooling boundary $n_e > n_0$ is cut out off the figure.

* * *

We thank the U.S. Department of Energy Office of Fusion Energy Sciences and Office of Advanced Scientific Computing Research for support under the Tokamak Disruption Simulation (TDS) Scientific Discovery through Advanced Computing (SciDAC) project, and the Base Theory Program, both at Los Alamos National Laboratory (LANL) under contract No. 89233218CNA000001. YZ was supported under a Director's Postdoctoral Fellowship at LANL. This research used resources of the National Energy Research Scientific Computing Center

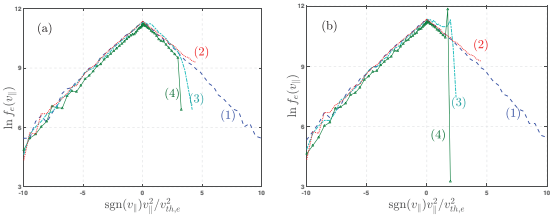

Fig. 4: Electron distributions at different locations. (a) is for the absorbing boundary and (b) is for the thermobath boundary. The positions are ahead of precooling front (1), between precooling and precooling trailing fronts (2), between recession and precooling trailing fronts (3) and within the recession layer (4). The parameters for the simulation with the thermobath boundary are the same as fig. 1 in the paper.

(NERSC), a U.S. Department of Energy Office of Science User Facility operated under Contract No. DE-AC02-05CH11231 and the Los Alamos National Laboratory Institutional Computing Program, which is supported by the U.S. Department of Energy National Nuclear Security Administration under Contract No. 89233218CNA000001.

Data availability statement: All data that support the findings of this study are included within the article (and any supplementary files).

Appendix

The electron distributions in $v_\parallel$ at different locations from the first-principle VPIC kinetic simulations as shown in fig. 4. In contrast to the absorbing boundary, there is a cold electron beam in f_e at the trap-passing boundary up to the precooling trailing front for the thermobath boundary, which causes a smaller cutoff velocity. This observation motivates the choice of eq. (5) in the paper as a model electron distribution to understand the electron transport physics underlying the thermal collapse of a nearly collisionless plasma.

REFERENCES

[1] National Research Council, *Plasma Science: Advancing Knowledge in the National Interest* (The National Academies Press, Washington, DC) 2007, ISBN 978-0-309-10943-7.

[2] Doyle E., Houlberg W., Kamada Y., Mukhovatov V., Osborne T., Polevoi A., Bateman G., Connor J., Cordey J. C., Fujita T., Garbet X., Hahm T., Horton L., Hubbard A., Imbeaux F., Jenko F., Kinsey J., Kishimoto Y., Li J., Luce T., Martin Y., Ossipenko M., Parail V., Peeters A., Rhodes T., Rice J., Roach C., Rozhansky V., Ryter F., Saibene G., Sartori R., Sips A., Snipes J., Sugihara M., Synakowski E., Takenaga H., Takizuka T., Thomsen K., Wade M. and Wilson H., ITPA Transport Physics Topical Group, ITPA Confinement Database and Modelling Topical Group and ITPA Pedestal and Edge Topical Group, *Nucl. Fusion*, **47** (2007) S18.

[3] Federici G., Bachmann C., Barucca L., Biel W., Boccaccini L., Brown R., Bustreo C., Ciattaglia S., Cismondi F., Coleman M., Corato V., Day C., Diegele E., Fischer U., Franke T., Gliss C., Ibarra A., Kembleton R., Loving A., Maviglia F., Meszaros B., Pintsuk G., Taylor N., Tran M., Vorpahl C., Wenninger R. and You J., *Fusion Eng. Des.*, **136** (2018) 729.

[4] Rodriguez-Fernandez P., Creely A., Greenwald M., Brunner D., Ballinger S., Chrobak C., Garnier D., Granetz R., Hartwig Z., Howard N., Hughes J., Irby J., Izzo V., Kuang A., Lin Y., Marmar E., Mumgaard R., Rea C., Reinke M., Riccardo V., Rice J., Scott S., Sorbom B., Stillerman J., Sweeney R., Tinguely R., Whyte D., Wright J. and Yuryev D., *Nucl. Fusion*, **62** (2022) 042003.

[5] Parks G., *Magnetosphere*, in *Encyclopedia of Atmospheric Sciences*, second edition, edited by North G. R., Pyle J. and Zhang F. (Academic Press, Oxford) 2015, pp. 309–315, ISBN 978-0-12-382225-3.

[6] Denton M. H., Borovsky J. E. and Cayton T. E., *J. Geophys. Res. Space Phys.*, **115** (2010) A01208.

[7] Denton M. H. and Cayton T. E., *Ann. Geophys.*, **29** (2011) 1755.

[8] Borovsky J. E., Cayton T. E., Denton M. H., Belian R. D., Christensen R. A. and Ingraham J. C., *J. Geophys. Res.: Space Phys.*, **121** (2016) 5449.

[9] Fabian A. C., *Annu. Rev. Astron. Astrophys.*, **32** (1994) 277.

[10] Fabian A. C., *Cooling flows in clusters of galaxies*, in *Lighthouses of the Universe: The Most Luminous Celestial Objects and Their Use for Cosmology*, edited by Gilfanov M., Sunyeav R. and Churazov E. (Springer, Berlin, Heidelberg) 2002, pp. 24–36, ISBN 978-3-540-48014-3.

[11] Peterson J. and Fabian A., *Phys. Rep.*, **427** (2006) 1.

[12] Aharonian F., Akamatsu H., Akimoto F., Allen S. W., Anabuki N., Angelini L., Arnaud K., Audard M., Awaki H., Axelsson M., Bamba A., Bautz M., Blandford R., Brenneman L., Brown G. V., Bulbul E., Cackett E., Chernyakova M., Chiao M., Coppi P., Costantini E., de Plaa J., den Herder J. W., Done C., Dotani T., Ebisawa K., Eckart M., Enoto T., Ezoe Y., Fabian A. C., Ferrigno C., Foster A., Fujimoto R., Fukazawa Y., Furuzawa A., Galeazzi M., Gallo L., Gandhi P., Giustini M., Goldwurm A., Gu L., Guainazzi M., Haba Y., Hagino K., Hamaguchi K., Harrus I., Hatsukade I., Hayashi K., Hayashi T., Hayashida K., Hiraga J., Hornschemeier A., Hoshino A., Hughes J., Iizuka R., Inoue H., Inoue Y., Ishibashi K., Ishida M., Ishikawa K., Ishisaki Y., Itoh M., Iyomoto N., Kaastra J., Kallman T., Kamae T., Kara E., Kataoka J., Katsuda S., Katsuta J., Kawaharada M., Kawai N., Kelley R., Khangulyan D., Kilbourne C., King A., Kitaguchi T., Kitamoto S., Kitayama T., Kohmura T., Kokubun M., Koyama S., Koyama K., Kretschmar P., Krimm H., Kubota A., Kunieda H., Laurent P., Lebrun F., Lee S. H., Leutenegger M., Limousin O., Loewenstein M., Long K. S., Lumb D., Madejski G., Maeda Y., Maier D., Makishima K., Markevitch M., Matsumoto H., Matsushita

K., McCammon D., McNamara B., Mehdipour M., Miller E., Miller J., Mineshige S., Mitsuda K., Mitsuishi I., Miyazawa T., Mizuno T., Mori H., Mori K., Moseley H., Mukai K., Murakami H., Murakami T., Mushotzky R., Nagino R., Nakagawa T., Nakajima H., Nakamori T., Nakano T., Nakashima S., Nakazawa K., Nobukawa M., Noda H., Nomachi M., O'Dell S., Odaka H., Ohashi T., Ohno M., Okajima T., Ota N., Ozaki M., Paerels F., Paltani S., Parmar A., Petre R., Pinto C., Pohl M., Porter F S., Pottschmidt K., Ramsey B., Reynolds C., Russell H., Safi-Harb S., Saito S., Sakai K., Sameshima H., Sato G., Sato K., Sato R., Sawada M., Schartel N., Serlemitsos P., Seta H., Shidatsu M., Simionescu A., Smith R., Soong Y., Stawarz L., Sugawara Y., Sugita S., Szymkowiak A., Tajima H., Takahashi H., Takahashi T., Takeda S., Takei Y., Tamagawa T., Tamura K., Tamura T., Tanaka T., Tanaka Y., Tanaka Y., Tashiro M., Tawara Y., Terada Y., Terashima Y., Tombesi F., Tomida H., Tsuboi Y., Tsujimoto M., Tsunemi H., Tsuru T., Uchida H., Uchiyama H., Uchiyama Y., Ueda S., Ueda Y., Ueno S., Uno S., Urry M., Ursino E., de Vries C., Watanabe S., Werner N., Wik D., Wilkins D., Williams B., Yamada S., Yamaguchi H., Yamaoka K., Yamasaki N Y., Yamauchi M., Yamauchi S., Yaqoob T., Yatsu Y., Yonetoku D., Yoshida A., Yuasa T., Zhuravleva I., Zoghbi A. and Hitomi Collaboration, *Nature*, **535** (2016) 117.

[13] Zhuravleva I., Churazov E., Schekochihin A. A., Allen S. W., Arévalo P., Fabian A. C., Forman W. R., Sanders J. S., Simionescu A., Sunyaev R., Vikhlinin A. and Werner N., *Nature*, **515** (2014) 85.

[14] Krolik J. K., *Active Galactic Nuclei: From the Central Black Hole to the Galatic Environment* (Princeton University Press, Princeton, N.J.) 1999.

[15] Hastings D. E. and Garrett H. B., *Spacecraft-Environment Interactions* (Cambridge University Press, Cambridge, UK) 1996.

[16] Nwankwo V. U., Jibiri N. N. and Kio M. T., *The impact of space radiation environment on satellites operation in near-earth space*, in *Satellites Missions and Technologies for Geosciences*, edited by Demyanov V. and Becedas J. (IntechOpen, Rijeka) 2020, Chapt 5.

[17] Federici G., Andrew P., Barabaschi P., Brooks J., Doerner R., Geier A., Herrmann A., Janeschitz G., Krieger K., Kukushkin A. *et al.*, *J. Nucl. Mater.*, **313** (2003) 11.

[18] Baylor L. R., Combs S. K., Foust C. R., Jernigan T. C., Meitner S., Parks P., Caughman J. B., Fehling D., Maruyama S., Qualls A. *et al.*, *Nucl. Fusion*, **49** (2009) 085013.

[19] Combs S. K., Meitner S. J., Baylor L. R., Caughman J. B., Commaux N., Fehling D. T., Foust C. R., Jernigan T. C., McGill J. M., Parks P. B. *et al.*, *IEEE Trans. Plasma Sci.*, **38** (2010) 400.

[20] Shiraki D., Commaux N., Baylor L. R., Eidietis N. W., Hollmann E. M., Lasnier C. J. and Moyer R. A., *Phys. Plasmas*, **23** (2016) 062516.

[21] Bondeson A., Parker R., Hugon M. and Smeulders P., *Nucl. Fusion*, **31** (1991) 1695.

[22] Riccardo V., Andrew P., Ingesson L. and Maddaluno G., *Plasma Phys. Control. Fusion*, **44** (2002) 905.

[23] Nardon E., Fil A., Hoelzl M., Huijsmans G. *et al.*, *Plasma Phys. Control. Fusion*, **59** (2016) 014006.

[24] Sweeney R., Choi W., Austin M., Brookman M., Izzo V., Knolker M., La Haye R., Leonard A., Strait E., Volpe F. *et al.*, *Nucl. Fusion*, **58** (2018) 056022.

[25] Riccardo V., Loarte A. *et al.*, *Nucl. Fusion*, **45** (2005) 1427.

[26] Arnoux G., Loarte A., Riccardo V., Fundamenski W., Huber A. and JET-EFDA contributors, *Nucl. Fusion*, **49** (2009) 085038.

[27] Braginskii S. I., *Reviews of Plasma Physics*, edited by Leontovich M. A., Vol. **I** (Consultants Bureau, New York) 1965, pp. 205–311.

[28] Atzeni S. and Meyer-Ter-Vehn J., *The Physics of Inertial Fusion* (Oxford University Press, Inc.) 2004.

[29] Bell A. R., *Phys. Fluids*, **28** (1985) 2007.

[30] Binney J. and Cowie L. L., *Astrophys. J.*, **247** (1981) 464.

[31] Fabian A. C., Nulsen P. E. J. and Canizares C. R., *Astron. Astrophys. Rev.*, **2** (1991) 191.

[32] Tribble P. C., *Mon. Not. R. Astron. Soc.*, **238** (1989) 1247.

[33] Chandran B. D. G. and Cowley S. C., *Phys. Rev. Lett.*, **80** (1998) 3077.

[34] Jafelice L. C., *Astron. J.*, **104** (1992) 1279.

[35] Balbus S. A. and Reynolds C. S., *Astrophys. J.*, **681** (2008) L65 (arXiv:0806.0940).

[36] Roberg-Clark G. T., Drake J. F., Reynolds C. S. and Swisdak M., *Phys. Rev. Lett.*, **120** (2018) 035101.

[37] Boozer A. H., *Phys. Fluids*, **19** (1976) 149.

[38] Boozer A. H., *Phys. Fluids*, **23** (1980) 2283.

[39] Park J. k., Boozer A. H. and Menard J. E., *Phys. Rev. Lett.*, **102** (2009) 065002.

[40] Yang S. M., Park J. K., Na Y. S., Wang Z. R., Ko W. H., In Y., Lee J. H., Lee K. D. and Kim S. K., *Phys. Rev. Lett.*, **123** (2019) 095001.

[41] Terry P. W., Fiksel G., Ji H., Almagri A. F., Cekic M., Den Hartog D. J., Diamond P. H., Prager S. C., Sarff J. S., Shen W., Stoneking M. and Ware A. S., *Phys. Plasmas*, **3** (1996) 1999.

[42] Bowers K. J., Albright B., Yin L., Bergen B. and Kwan T., *Phys. Plasmas*, **15** (2008) 055703.

[43] Allen J. and Andrews J., *J. Plasma Phys.*, **4** (1970) 187.

[44] Cipolla J. and Silevitch M., *J. Plasma Phys.*, **25** (1981) 373.

[45] Guo Z. and Tang X. Z., *Phys. Plasmas*, **19** (2012) 082310.

[46] Guo Z., Tang X. Z. and McDevitt C., *Phys. Plasmas*, **21** (2014) 102512.

[47] Li Y., Srinivasan B., Zhang Y. and Tang X. Z., *Phys. Rev. Lett.*, **128** (2022) 085002.

[48] Li Y., Srinivasan B., Zhang Y. and Tang X. Z., *Phys. Plasmas*, **29** (2022) 113509.

[49] Tang X. Z. and Guo Z., *Phys. Plasmas*, **23** (2016) 083503.

[50] Tang X. Z. and Guo Z., *Phys. Plasmas*, **23** (2016) 120701.